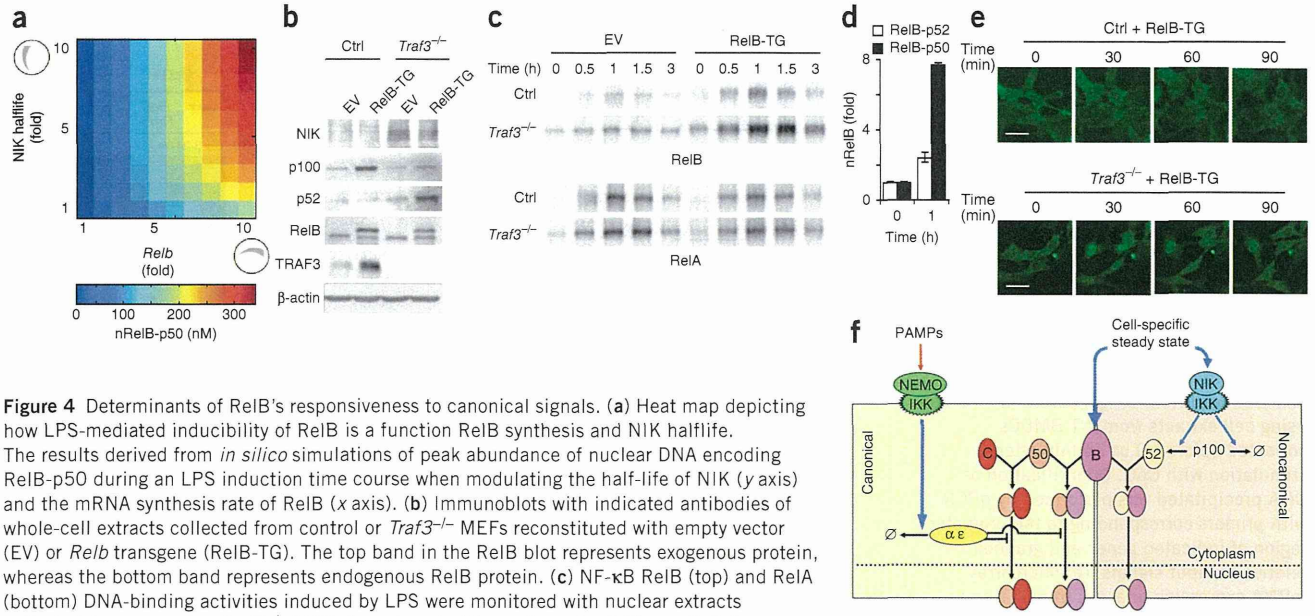

Figure 4 Determinants of RelB's responsiveness to canonical signals. (**a**) Heat map depicting how LPS-mediated inducibility of RelB is a function RelB synthesis and NIK halflife. The results derived from *in silico* simulations of peak abundance of nuclear DNA encoding RelB-p50 during an LPS induction time course when modulating the half-life of NIK (*y* axis) and the mRNA synthesis rate of RelB (*x* axis). (**b**) Immunoblots with indicated antibodies of whole-cell extracts collected from control or *Traf3*$^{-/-}$ MEFs reconstituted with empty vector (EV) or *Relb* transgene (RelB-TG). The top band in the RelB blot represents exogenous protein, whereas the bottom band represents endogenous RelB protein. (**c**) NF-κB RelB (top) and RelA (bottom) DNA-binding activities induced by LPS were monitored with nuclear extracts collected from control or *Traf3*$^{-/-}$ MEFs transduced with empty vector (EV) or a *Relb* transgene (RelB-TG). (**d**) Quantification of nuclear (n)RelB-p50 and RelB-p52 activities in LPS-stimulated *Traf3*$^{-/-}$ (*Relb* transgene) MEFs; signals were graphed relative to respective RelB-containing dimers' basal activity. (**e**) Single-cell data at indicated time points[7] of the nuclear localization of a retrovirally expressed RelB-GFP fusion protein in response to TNF stimulation of control or *Traf3*$^{-/-}$ MEFs (RelB-TG). Scale bars, 10 μm. (**f**) Schematic depicting the regulation of RelB by noncanonical or canonical stimuli. RelB may either dimerize with p52 in response to stimulus-induced noncanonical stimuli or dimerize with p50 and become responsive to canonical stimuli. Cell type–specific steady-state control of RelB expression and noncanonical pathway activity determines which stimuli activate RelB: at low steady-state levels, RelB is responsive to noncanonical stimuli as reported in MEFs; at high steady-state levels RelB will dimerize not only p52 but also p50, and becomes responsive to canonical stimuli via IκBα and IκBε control. Data shown here are representative of two independent experiments (error bars, s.d.; $n = 3$).

observed rapid activation of RelB in splenic DCs stimulated with CpG or Pam_3CSK_4 (**Supplementary Fig. 3d**). Computational simulations suggested that this induced RelB activity consists of RelB-p50 rather than RelB-p52 dimer (**Fig. 3c**). Experimentally, supershift analyses of nuclear extracts revealed that both RelB-p50 and RelB-p52 activities were present under unstimulated conditions but that CpG stimulation primarily increased RelB-p50 activity (**Fig. 3c** and **Supplementary Fig. 3e**), unlike LTßR stimulation of MEFs, which induces RelB-p52. These data suggest that during DC maturation RelB activation is regulated by the canonical pathway.

A hallmark of canonical signaling is the release of a pre-existing NF-κB dimer, whereas noncanonical signaling involves the stimulus-responsive *de novo* generation of the dimer[12,25]. In CpG-responding DCs we did not detect increases in protein expression of RelB or p50, or *Relb* mRNA, whereas *Nfkbia* mRNA, encoding IκBα, was induced more than fourfold (**Supplementary Fig. 3f**). Furthermore, inhibition of protein synthesis by cycloheximide did not block CpG-induced RelB activation, whereas resynthesis of IκBα protein was blocked (**Supplementary Fig. 3g**), suggesting that *de novo* RelB protein synthesis is not required for CpG-inducible RelB activation. In contrast, immunoblotting confirmed that in DCs nuclear accumulation of RelB was accompanied by disappearance of cytoplasmic RelB after CpG stimulation, indicative of stimulus-responsive nuclear translocation of a pre-existing pool of RelB (**Supplementary Fig. 3h**). Inhibition of IKK2 activity, a hallmark of the canonical pathway, by the inhibitor PS-1145 (ref. 26) resulted not only in reduced RelA activity and IκBα protein degradation but also in reduced RelB activation (**Supplementary Fig. 3g,i**), suggesting that IKK2 signaling is required for RelB activation. We monitored the abundance of known NF-κB inhibitor proteins during the CpG time course: the abundance of the potential RelB inhibitors p100 and p105 remained unaltered; however, IκBα and IκBε were rapidly degraded, correlating with the activation kinetics of RelB activation (**Fig. 3d**). Notably, in coimmunoprecipitation assays, the amount of IκBα associated with RelB decreased in response to CpG (**Fig. 3e**). Together, these data suggest that degradation of IκBα allows for the release of RelB from pre-existing IκBα-RelB complexes.

To investigate the role of IκBα in TLR-induced RelB activation, we used the mathematical model to computationally simulate the effect of IκB deletions on RelB activation. We found that *in silico* deletion of individual inhibitors had little effect, except in the case of IκBα (**Supplementary Fig. 3j**). Even compound deficiency of IκBβ, IκBε and IκBδ (which elevated basal RelB activity; **Supplementary Fig. 3k**) showed robust RelB activation in response to canonical pathway activation, as opposed to greatly diminished activation in an IκBα-deficient model (**Fig. 3f**). To test these computational modeling predictions, we used IκBα-deficient mice[22] and generated *Nfkbib*$^{-/-}$*Nfkbie*$^{-/-}$*Nfkb2*$^{-/-}$ mice. We confirmed the lack of protein products by immunoblotting (**Supplementary Fig. 3l**). Indeed, RelB activation was robust in *Nfkbib*$^{-/-}$*Nfkbie*$^{-/-}$*Nfkb2*$^{-/-}$ BMDCs, whereas IκBα-deficient BMDCs showed a diminished increase and delayed kinetics (**Fig. 3g** and **Supplementary Fig. 3m**). Together, these data provide genetic and mechanistic evidence that IκBα is required for CpG-induced RelB activation in DCs.

Engineered MEFs show DC-like RelB control

We previously showed that hallmarks of the NF-κB signaling system in mature but unstimulated DCs are abundant in basal RelB expression

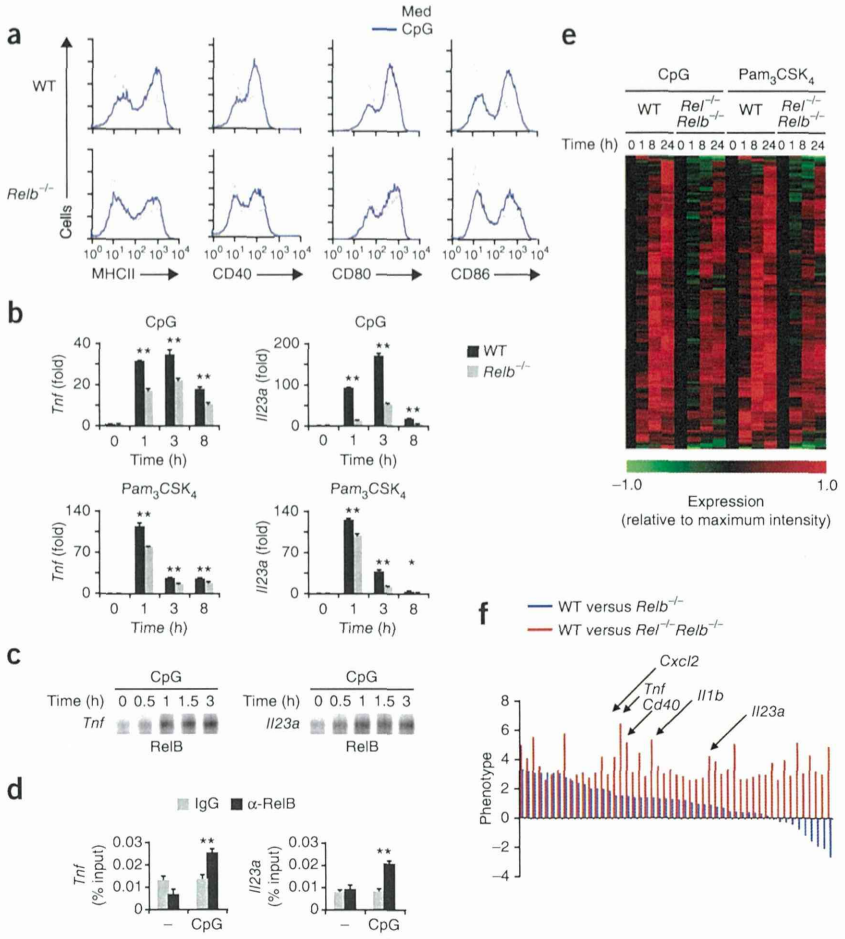

Figure 5 RelB regulates DC activation markers and inflammatory mediators. (**a**) Analysis of cell surface marker expression in wild-type (WT) and *Relb*$^{-/-}$ BMDCs in response to CpG. Cells untreated (Med) or treated with CpG for 24 h were analyzed by FACS. (**b**) Gene expression analyses of WT and *Relb*$^{-/-}$ BMDCs stimulated with CpG or Pam_3CSK_4 for the indicated time course by qRT-PCR. Signals were graphed relative to respective resting cells. (**c**) EMSA with nuclear extracts collected from CpG-stimulated WT BMDCs using DNA probes containing the κB site containing promoter sequence from *Tnf* or *Il23a* gene. (**d**) Chromatin immunoprecipitation analyses with RelB or IgG control antibodies using cell extracts from WT BMDCs collected before (–) or 75 min after stimulation with CpG. Quantification of DNA precipitated was performed by qPCR with primers corresponding to the promoter region of indicated genes and graphed relative to input signals. (**e**) Microarray mRNA expression analysis from WT and *Rel*$^{-/-}$*Relb*$^{-/-}$ BMDCs stimulated with CpG and Pam_3CSK_4 for indicated time points. Heat map shows the expression pattern from one experiment in a (log_2) fold induction scale of 157 significant downregulated genes in *Rel*$^{-/-}$*Relb*$^{-/-}$ BMDCs identified by significant analysis of microarray (SAM). Color scale '1.0' denotes normalized highest expression value of the given gene across time courses. (**f**) RelB and c-Rel regulate overlapping sets of genes. The expression phenotype caused by RelB deficiency was determined for the 50 genes with the most severe expression defect in *Rel*$^{-/-}$*Relb*$^{-/-}$ BMDCs. The list of genes was sorted according to expression differences between WT and *Relb*$^{-/-}$ BMDCs. Data shown in **a**–**d** are representative of at least three independent experiments (error bars, s.e.m.; $n = 3$). $^*P < 0.05$ and $^{**}P < 0.01$.

and basal noncanonical pathway activity. To investigate whether these mechanisms are sufficient and what their relative contributions may be, we performed computational simulations of RelB activation for a range of parameter values governing basal *Relb* mRNA synthesis and NIK protein half-life. These *in silico* analyses showed that activation of RelB mildly increased when either parameter was increased, but substantial enhancement occurred only when both parameters were concomitantly elevated (**Fig. 4a**). Our simulations suggest that the DC-specific, rapid RelB activation upon canonical pathway stimulation can be explained by DC-specific, constitutively elevated *Relb* mRNA synthesis and noncanonical IKK activity.

To test this model-derived hypothesis experimentally, we asked whether genetically engineering these two mechanisms into MEFs may be sufficient to allow for DC-like canonical regulation of RelB. We took advantage of MEFs deficient in TRAF3, an E3-ligase controlling NIK degradation[27], to increase constitutive noncanonical signaling. As suggested by the model simulations, we then transduced a retroviral *Relb* transgene to increase RelB expression about threefold relative to that in untransduced MEFs (**Fig. 4b** and **Supplementary Fig. 4a**). The engineered MEFs exhibited substantial RelB activation in response to LPS (**Fig. 4c**) or TNF (**Supplementary Fig. 4b**), whereas the parental control MEFs did not, and RelA activation by these stimuli remained unchanged. Neither single genetic alteration produced substantial RelB activation, indicating that enhanced RelB expression and noncanonical pathway activity function synergistically, as predicted by the model, to push RelB into the canonical pathway and render it responsive to TLR agonists. Antibody supershift and depletion analysis (**Fig. 4d** and **Supplementary Fig. 4c**) confirmed that canonical signaling primarily activated the RelB-p50 dimer (sevenfold) rather than the RelB-p52 dimer (twofold) as observed in DCs and predicted by the computational model (**Fig. 3c**). Overexpression of a RelB-GFP fusion protein retrovirally transduced into single cells also revealed nuclear translocation upon TNF stimulation in the *Traf3*$^{-/-}$ context but not in control cells (**Fig. 4e**).

These iterative computational-experimental studies support a model in which the NF-κB protein RelB may function in either noncanonical or canonical pathways (**Fig. 4f**). In a dimer with p100 or p52, RelB is subject to control by the noncanonical pathway; in a dimer with p50, RelB may be bound by IκBα and IκBε and is regulated by NEMO-dependent canonical signals. Our analysis indicates that low constitutive RelB expression and noncanonical pathway activity characterizes one steady state (found in MEFs) and allows for RelB-p52 activation by stimuli such as LTβ that engage the noncanonical pathway (**Supplementary Fig. 4d**). High constitutive RelB expression and noncanonical pathway activity characterize another steady state (found in DCs) and allow for RelB-p50 activation by stimuli such as CpG that engage the canonical pathway (**Supplementary Fig. 4e**).

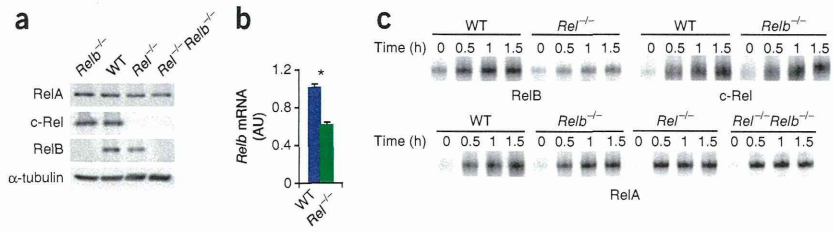

Figure 6 RelB may mediate cRel functions in DCs. (**a**) Immunoblot for RelA, RelB and c-Rel of whole-cell extracts prepared from indicated BMDCs. α-tubulin served as a loading control. (**b**) Amount of *Relb* transcripts compared by quantitative RT-PCR with mRNA collected from wild-type and $Rel^{-/-}$ BMDCs, relative to wild-type (WT) cells. (**c**) NF-κB DNA binding activities of RelB, c-Rel and RelA induced by LPS in indicated gene-deficient BMDCs monitored by EMSA. Data shown are representative of three independent experiments (error bars, s.e.m.; $n = 4$). $^*P < 0.01$.

RelB and c-Rel cooperate in TLR-induced DC maturation

Given that RelB-p50 is induced by PAMPs during DC maturation, we wondered whether it controls the expression of inflammatory regulators or DC activation markers. After stimulation with the TLR9 ligand CpG or the TLR2 ligand Pam_3CSK_4 for 24 h, we indeed observed reduced surface expression of DC activation markers MHCII, CD86, CD80 and CD40 in $Relb^{-/-}$ DCs (**Fig. 5a** and **Supplementary Fig. 5a,b**). Expression of proinflammatory genes, *Tnf* and *Il23a*, correlated with the kinetics of CpG or Pam_3CSK_4-induced RelB activation and were reduced in $Relb^{-/-}$ DCs (**Fig. 5b**). In EMSAs, activated RelB-p50 bound to DNA probes containing the κB sites found in the *Tnf* and *Il23a* promoters (**Fig. 5c**), indicating that RelB-p50 can directly interact with these regulatory regions. *In vivo*, we observed recruitment of RelB to the promoter regions of *Tnf* and *Il23a* genes after DC maturation with CpG using the chromatin immunoprecipitation assay (**Fig. 5d**).

We noted that RelB bound to consensus κB site sequences[28] associated with the known canonical NF-κB pathway effectors, RelA and c-Rel, rather than the unconventional sequences previously ascribed to RelB in splenic stromal cells[29] or MEFs[20]. Because single knockouts did not show overt defects in $CD11c^+$ cell generation in bone marrow cultures (**Supplementary Fig. 5d**), we tested whether c-Rel and RelB have overlapping functions in regulating the DC maturation program by examining gene expression in c-Rel and RelB doubly-deficient DCs. Genome-wide expression profiling activated by TLR ligands CpG and Pam_3CSK_4 revealed a group of 157 genes that were substantially downregulated in $Rel^{-/-}Relb^{-/-}$ BMDCs (**Fig. 5e** and **Supplementary Table 1**). To delineate the contribution of RelB in activating these genes, we examined the expression phenotype of the 50 most severely c-Rel–RelB-dependent genes in $Relb^{-/-}$ BMDCs stimulated with TLR ligands. Expression phenotypes in fold induction were calculated between wild-type and null DCs, and the order of genes was sorted in increasing degree of RelB dependency (**Fig. 5f** and **Supplementary Table 2**). This analysis revealed a continuous spectrum of RelB dependency rather than two distinct classes (of RelB-dependent and RelB-independent genes), suggesting an overlap in DNA interaction specificities between c-Rel and RelB dimers. *Tnf* and *Il23a* were identified in this analysis as regulated by both RelB and c-Rel. Quantitative RT-PCR validated the requirements of RelB and c-Rel in activating *Cxcl2*, *Cd40* and *Il1b* gene expression (**Supplementary Fig. 5c**).

Given overlapping functions of c-Rel and RelB in regulating DC gene expression programs, we investigated their relationship within the signaling system. Whereas RelA and c-Rel protein expression were similarly abundant in wild-type BMDCs and those lacking RelB, $Rel^{-/-}$ BMDCs exhibited decreased RelB protein expression (**Fig. 6a**). *Relb* transcripts were reduced by ~40% in $Rel^{-/-}$ relative to wild-type BMDC (**Fig. 6b**). This reduction resulted in severely diminished activation of RelB DNA-binding activity in $Rel^{-/-}$ BMDCs in response to LPS (**Fig. 6c**). These data indicate that one of the key determinants of RelB control by the canonical pathway, namely RelB expression, is in fact controlled by c-Rel. The feed-forward circuit architecture suggests that expression of RelB in differentiated but immature DCs may reflect the exposure of differentiating cells to c-Rel–inducing stimuli. We therefore tested whether c-Rel–deficient DCs may also be defective in RelB-responsive gene expression by comparing the expression of RelB target genes in $Rel^{-/-}$ DCs and $Rel^{-/-}Relb^{-/-}$ DCs. Indeed, $Rel^{-/-}$ BMDCs showed reductions of surface marker and inflammatory cytokine expression (**Supplementary Fig. 6a,b**). These data support a model in which RelB acts as a downstream mediator of c-Rel in DC activation programs.

DISCUSSION

RelA and c-Rel had been previously considered as effectors of the canonical NF-κB signaling pathway, and RelB as the effector of the noncanonical pathway, based on its role as a RelB-p52 transcription factor in secondary lymphoid organogenesis. However, we showed here that RelB is also an effector of the canonical pathway in DCs. During DC differentiation RelB expression increased, and elevated steady-state noncanonical pathway activity resulted not only in the expected RelB-p52 dimer but in formation of the RelB-p50 dimer. Unlike RelB-p52, which is mostly nuclear in immature DCs, RelB-p50 is inhibited by the IκB proteins, IκBα and IκBε, which allows for rapid activation of RelB-p50 activity via the canonical pathway upon exposure to maturation stimuli. Conversely, with the recent discovery of IκBδ[21,22], chronic inflammatory conditions rendered RelA an effector of the noncanonical signaling pathway. Thus, both RelA and RelB are potential effectors of the canonical and noncanonical signaling pathways; whether they are functionally relevant effectors is determined by the physiological steady state of the NF-κB signaling system.

Our observations imply that RelB-p50 and RelB-p52 present different molecular surfaces to IκB proteins, providing physiological relevance to previous studies of protein-interaction specificities[30,31]. Similarly, the DNA interaction characteristics of RelB-p50 and RelB-p52 may be distinct[32,33]. RelB residue Arg125 in the RelB-p52 dimer makes an additional base contact with DNA that allows RelB-p52 to recognize a broader range of κB sites. This may account for the RelB-p52–specific function in regulating chemokines involved in secondary lymphoid organogenesis, such as secondary lymphoid tissue chemokine (SLC), EBI1 ligand chemokine (ELC), B lymphoblastoid cell chemokine (BLC) and stromal cell–derived factor 1α (SDF-1α)[20,29]. In contrast, RelB-p50 interacts with DNA sequences similarly to RelA-p50, and a role for RelB in TNF production, GM-CSF and Bcl-xl expression has been reported[34,35]. Together, these studies suggest that the dimerization partner of RelB determines not only the signaling pathway that RelB is responsive to but also the RelB target gene program.

Why then, would DCs use RelB as an effector of the canonical NF-κB signaling pathway along with RelA and c-Rel? One possibility

is that RelB-p50 target genes are distinct from those controlled by c-Rel or RelA. Our transcriptomic profiling suggests overlap between c-Rel–dependent and RelB-dependent gene programs, but c-Rel turned out to control RelB expression; thus, other tools are required to address the question of RelB-p50 versus cRel-p50 specificity. A second possibility is that the stimulus-responsive dynamic control of RelB is distinct from that of RelA or c-Rel. Although RelB-p50 is inhibited by IκBα in resting cells, it may make for a poorer substrate for IκB feedback control than RelA, which is efficiently stripped off the DNA by IκBα[36]. We speculate that the involvement of RelB-p50 in DC biology ensures irreversible execution of a terminal maturation and activation program in response to transient PAMP exposure.

Mathematical modeling, which we used here to describe biochemical reactions in terms of kinetic rate equations, lends itself as a tool for studying the regulation of signaling networks. Iteratively refined mathematical models of the NF-κB–IκB system have addressed the dynamic and homeostatic control of the NF-κB RelA-p50 dimer by IκB proteins in fibroblasts[21,22,37–41]. In this study, we developed to our knowledge the first kinetic model that accounts for the generation and regulation of multiple NF-κB dimers, namely RelA- and RelB- containing dimers. We contrasted the steady-state and dynamic control mechanisms in two cell types, MEFs and DCs, and found that the key biochemical differences are two kinetic rate constants (*Relb* mRNA synthesis and NIK half-life); a threefold increase was sufficient to shift the *in silico* model from MEF-like to DC-like regulation of the NF-κB signaling system. We confirmed this prediction experimentally by genetically engineering MEFs to produce DC-like RelB control. There was no need to invoke cell type–specific protein interaction specificities or any other cell type–specific molecular mechanism. The results indicate that cell type–specific quantitative control of the steady state of a signaling system may determine seemingly qualitative cell type–specific properties, such as DC-specific RelB activation by TLRs. As such, kinetic modeling and a quantitative analysis of signaling systems may serve to generate hypotheses not only for mechanistic studies but also for the development of DC-mediated therapeutics.

METHODS

Methods and any associated references are available in the online version of the paper.

Accession codes. GEO: microarray data, GSE34990.

Note: Supplementary information is available in the online version of the paper.

ACKNOWLEDGMENTS

We thank Z. Tao and G. Ghosh (University of California San Diego) for plasmids and recombinant proteins, S. Basak, A. Wu, P. Loriaux, R. Tsui for computational modeling advice, and C. Brown and M. Karin (University of California San Diego) for *Traf3*$^{-/-}$ embryos. This study was supported by GM085763 (A.H.), GM071573 (A.H.), AI090935 (A.H.), GM085325 (J.P.) and AI081923 (E.I.Z.).

AUTHOR CONTRIBUTIONS

V.F.-S.S. and A.H. designed the study. V.F.-S.S. and M.M. carried out all experimental work with assistance from J.Q.H., T.Y., R.F. and M.A., and guidance from E.I.Z. and A.H. J.D.-T. and J.D.K. carried out the computational modeling work and J.P. the bioinformatic analysis. V.F.-S.S. and A.H. wrote the manuscript with contributions from all authors.

COMPETING FINANCIAL INTERESTS

The authors declare no competing financial interests.

Published online at http://www.nature.com/doifinder/10.1038/ni.2446.
Reprints and permissions information is available online at http://www.nature.com/reprints/index.html.

1. Banchereau, J. & Steinman, R.M. Dendritic cells and the control of immunity. *Nature* **392**, 245–252 (1998).
2. Liu, Y.J. IPC: professional type 1 interferon-producing cells and plasmacytoid dendritic cell precursors. *Annu. Rev. Immunol.* **23**, 275–306 (2005).
3. Serbina, N.V., Salazar-Mather, T.P., Biron, C.A., Kuziel, W.A. & Pamer, E.G. TNF/iNOS-producing dendritic cells mediate innate immune defense against bacterial infection. *Immunity* **19**, 59–70 (2003).
4. Steinman, R.M. & Banchereau, J. Taking dendritic cells into medicine. *Nature* **449**, 419–426 (2007).
5. Carrasco, D., Ryseck, R.P. & Bravo, R. Expression of relB transcripts during lymphoid organ development: specific expression in dendritic antigen-presenting cells. *Development* **118**, 1221–1231 (1993).
6. Zanetti, M., Castiglioni, P., Schoenberger, S. & Gerloni, M. The role of relB in regulating the adaptive immune response. *Ann. NY Acad. Sci.* **987**, 249–257 (2003).
7. Li, M. *et al.* Immune modulation and tolerance induction by RelB-silenced dendritic cells through RNA interference. *J. Immunol.* **178**, 5480–5487 (2007).
8. Wu, L. *et al.* RelB is essential for the development of myeloid-related CD8α- dendritic cells but not of lymphoid-related CD8α^{+} dendritic cells. *Immunity* **9**, 839–847 (1998).
9. Kobayashi, T. *et al.* TRAF6 is a critical factor for dendritic cell maturation and development. *Immunity* **19**, 353–363 (2003).
10. Hofmann, J., Mair, F., Greter, M., Schmidt-Supprian, M. & Becher, B. NIK signaling in dendritic cells but not in T cells is required for the development of effector T cells and cell-mediated immune responses. *J. Exp. Med.* **208**, 1917–1929 (2011).
11. Yang, H. *et al.* Suppression of ongoing experimental autoimmune myasthenia gravis by transfer of RelB-silenced bone marrow dentritic cells is associated with a change from a T helper Th17/Th1 to a Th2 and FoxP3^{+} regulatory T-cell profile. *Inflamm. Res.* **59**, 197–205 (2010).
12. Pomerantz, J.L. & Baltimore, D. Two pathways to NF-κB. *Mol. Cell* **10**, 693–695 (2002).
13. Oeckinghaus, A., Hayden, M.S. & Ghosh, S. Crosstalk in NF-κB signaling pathways. *Nat. Immunol.* **12**, 695–708 (2011).
14. Derudder, E. *et al.* RelB/p50 dimers are differentially regulated by tumor necrosis factor-alpha and lymphotoxin-beta receptor activation: critical roles for p100. *J. Biol. Chem.* **278**, 23278–23284 (2003).
15. Lind, E.F. *et al.* Dendritic cells require the NF-κB2 pathway for cross-presentation of soluble antigens. *J. Immunol.* **181**, 354–363 (2008).
16. O'Sullivan, B.J. & Thomas, R. CD40 ligation conditions dendritic cell antigen-presenting function through sustained activation of NF-κB. *J. Immunol.* **168**, 5491–5498 (2002).
17. Saccani, S., Pantano, S. & Natoli, G. Modulation of NF-κB activity by exchange of dimers. *Mol. Cell* **11**, 1563–1574 (2003).
18. Ammon, C., Mondal, K., Andreesen, R. & Krause, S.W. Differential expression of the transcription factor NF-κB during human mononuclear phagocyte differentiation to macrophages and dendritic cells. *Biochem. Biophys. Res. Commun.* **268**, 99–105 (2000).
19. Gasparini, C., Foxwell, B.M. & Feldmann, M. RelB/p50 regulates CCL19 production, but fails to promote human DC maturation. *Eur. J. Immunol.* **39**, 2215–2223 (2009).
20. Basak, S., Shih, V.F. & Hoffmann, A. Generation and activation of multiple dimeric transcription factors within the NF-κB signaling system. *Mol. Cell. Biol.* **28**, 3139–3150 (2008).
21. Basak, S. *et al.* A fourth IκB protein within the NF-κB signaling module. *Cell* **128**, 369–381 (2007).
22. Shih, V.F. *et al.* Kinetic control of negative feedback regulators of NF-κB/RelA determines their pathogen- and cytokine-receptor signaling specificity. *Proc. Natl. Acad. Sci. USA* **106**, 9619–9624 (2009).
23. Li, T. *et al.* MicroRNAs modulate the noncanonical transcription factor NF-κB pathway by regulating expression of the kinase IKKα during macrophage differentiation. *Nat. Immunol.* **11**, 799–805 (2010).
24. Wuerzberger-Davis, S.M. *et al.* Nuclear export of the NF-κB inhibitor IκBα is required for proper B cell and secondary lymphoid tissue formation. *Immunity* **34**, 188–200 (2011).
25. Shih, V.F., Tsui, R., Caldwell, A. & Hoffmann, A. A single NFκB system for both canonical and non-canonical signaling. *Cell Res.* **21**, 86–102 (2011).
26. Waterfield, M., Jin, W., Reiley, W., Zhang, M. & Sun, S.C. IκB kinase is an essential component of the Tpl2 signaling pathway. *Mol. Cell. Biol.* **24**, 6040–6048 (2004).
27. He, J.Q. *et al.* Rescue of TRAF3-null mice by p100 NF-κB deficiency. *J. Exp. Med.* **203**, 2413–2418 (2006).
28. Hoffmann, A., Natoli, G. & Ghosh, G. Transcriptional regulation via the NF-κB signaling module. *Oncogene* **25**, 6706–6716 (2006).
29. Bonizzi, G. *et al.* Activation of IKKα target genes depends on recognition of specific κB binding sites by RelB:p52 dimers. *EMBO J.* **23**, 4202–4210 (2004).
30. Lernbecher, T., Kistler, B. & Wirth, T. Two distinct mechanisms contribute to the constitutive activation of RelB in lymphoid cells. *EMBO J.* **13**, 4060–4069 (1994).
31. Dobrzanski, P., Ryseck, R.P. & Bravo, R. Differential interactions of Rel-NF-κB complexes with IκBα determine pools of constitutive and inducible NF-κB activity. *EMBO J.* **13**, 4608–4616 (1994).

32. Fusco, A.J. *et al.* NF-κB p52:RelB heterodimer recognizes two classes of κB sites with two distinct modes. *EMBO Rep.* **10**, 152–159 (2009).
33. Moorthy, A.K., Huang, D.B., Wang, V.Y., Vu, D. & Ghosh, G. X-ray structure of a NF-κB p50/RelB/DNA complex reveals assembly of multiple dimers on tandem κB sites. *J. Mol. Biol.* **373**, 723–734 (2007).
34. Weih, F., Warr, G., Yang, H. & Bravo, R. Multifocal defects in immune responses in RelB-deficient mice. *J. Immunol.* **158**, 5211–5218 (1997).
35. Sasaki, C.Y., Ghosh, P. & Longo, D.L. Recruitment of RelB to the Csf2 promoter enhances RelA-mediated transcription of granulocyte-macrophage colony-stimulating factor. *J. Biol. Chem.* **286**, 1093–1102 (2011).
36. Bergqvist, S. *et al.* Kinetic enhancement of NF-κBxDNA dissociation by IκBα. *Proc. Natl. Acad. Sci. USA* **106**, 19328–19333 (2009).
37. Werner, S.L., Barken, D. & Hoffmann, A. Stimulus specificity of gene expression programs determined by temporal control of IKK activity. *Science* **309**, 1857–1861 (2005).
38. O'Dea, E.L., Kearns, J.D. & Hoffmann, A. UV as an amplifier rather than inducer of NF-κB activity. *Mol. Cell* **30**, 632–641 (2008).
39. O'Dea, E.L. *et al.* A homeostatic model of IκB metabolism to control constitutive NF-κB activity. *Mol. Syst. Biol.* **3**, 111 (2007).
40. Kearns, J.D., Basak, S., Werner, S.L., Huang, C.S. & Hoffmann, A. IκBepsilon provides negative feedback to control NF-κB oscillations, signaling dynamics, and inflammatory gene expression. *J. Cell Biol.* **173**, 659–664 (2006).
41. Hoffmann, A., Levchenko, A., Scott, M.L. & Baltimore, D. The IκB-NF-κB signaling module: temporal control and selective gene activation. *Science* **298**, 1241–1245 (2002).

ONLINE METHODS

Reagents. GM-CSF and IL-4 were from Peprotech. We used 0.1 μM CpG (Invivogen), 500 ng/ml Pam3CSK4 (Invivogen), 100 ng/ml LPS (Sigma, B5:055) and 0.5 μg/ml LTβR agonist (Biogen) to stimulate cells. Cycloheximide and IKK2 inhibitor (PS-1145) were from Sigma. Antibodies to RelA (sc-372), RelB (sc-226), c-Rel (sc-70), IκBα (sc-371), IκBβ (sc-945), IκBε (sc-7155), IKK1 (sc-7606), TRAF3 (sc-6933), USF-2 (sc-861), α-tubulin (sc-5286), β-actin (sc-1615) and CD16/CD32 (sc-18867) were from Santa Cruz Biotechnology. p105/p50, p100/p52 and antibody to p100 C terminus were from US National Cancer Institute, Biological Resources Branch, Frederick, Maryland, USA. NIK antibody (4994) was from Cell Signaling. Immunoprecipitation beads and HRP-conjugated anti-rabbit secondary antibody (18-8816) were from eBioscience.

Animals and cell culture. Wild-type and gene-deficient C57BL/6 mice were maintained in specific pathogen–free condition at the University of California, San Diego. All procedures were approved by the Institutional Animal Care and Use Committee of the University of California, San Diego. *Nfkbia*$^{-/-}$*Tnf*$^{-/-}$*Rel*$^{-/-}$ and *Nfkbia*$^{-/-}$*Tnf*$^{-/-}$ *Rel*$^{-/-}$*Relb*$^{-/-}$ mice were generated by cross-breeding *Nfkbia*$^{-/-}$*Tnf*$^{-/-}$ with *Rel*$^{-/-}$ and *Relb*$^{-/-}$ mice. *Nfkbib*$^{-/-}$*Nfkbie*$^{-/-}$*Nfkb2*$^{-/-}$ mice were generated by cross-breeding *Nfkbib*$^{-/-}$, *Nfkbie*$^{-/-}$ and *Nfkb2*$^{-/-}$ mice. *Rel*$^{-/-}$*Relb*$^{-/-}$ mice were generated by cross-breeding *Rel*$^{-/-}$ and *Relb*$^{-/-}$ mice. Primary MEFs were generated from E12.5–14.5 embryos. BMDMs and BMDCs were made from bone-marrow suspensions prepared from mouse femurs. We seeded 2 × 10^6 bone marrow cells on 10-cm plate and cultured them for one week with L929-conditioned DMEM to derive BMDMs or cultured them for 6–11 d with 20 ng/ml GM-CSF and 10 ng/ml IL-4 to derive BMDCs. BMDC medium was replaced on days 3, 6 and 8, and floating cells were collected and subjected to experimental analyses as previously described[42]. Typically, day 6–7 BMDCs were used to investigate TLR-induced DC maturation, and day 9–11 BMDCs for spontaneous DC maturation studies.

Splenic DC purification. Spleens were cut into small fragments and digested with collagenase D (2 mg/ml, Roche) for 30 min at 37 °C followed by incubation with 10 mM EDTA pH 8.0 for 5 min. Single-cell suspension of splenocytes were enriched for CD11c$^+$ cells by immunomagnetic cell sorting using MACS CD11c microbeads (Miltenyi Biotec) according to manufacturer's protocol.

Antibody staining and flow cytometry. Single-cell suspensions were collected and blocked with anti-mouse CD16/CD32 in PBS containing 5% FCS for 10 min. Cells were stained with 7-amino-actinomycin D (7-AAD) to exclude dead cells and indicated antibodies for DC maturation analyses. All antibodies were purchased from BD Pharmingen: anti-CD11 (HL3), anti-CD40 (3/23), anti-CD80 (16-10A1), anti-CD86 (GL-1) and anti-IA^b (AF6-120.1). Stained cells were acquired in either a FACSCalibur (BD Biosciences) or an Accuri C6 and data analysis was performed with FlowJo software.

Antigen presentation in DC–T cell cocultures. GM-CSF–derived bone marrow DCs were pulsed with 200 μg whole ovalbumin (Sigma, 5 μM OVA 323-339 (OT-II) peptide (Anaspec) or medium alone for 2 h at 37 °C. Naive CD4$^+$ T cells (5 × 10^4 cells/well) were obtained by negative enrichment (>90% purity; Stem Cell Technologies) from spleens of B6.Cg-Tg (*TcraTcrb*)425 Cbn/J mice transgenic for ovalbumin 323-339–specific αβTCR (Jackson Laboratory) and labeled with carboxyfluorescein succinimidyl ester (CFSE) (Sigma). DCs were washed and cultured with CFSE-labeled CD4$^+$ T cells (5 × 10^4 T cells/well) at the indicated DC:T cell ratios as described[43]. T cells were restimulated 72 h later with 5 μM OT-II peptide for 5 h in the presence of brefeldin A and examined for CFSE dilution and production of TNF and IL-2 by flow cytometry (BD LSRII). Data were analyzed using FlowJo software (Treestar).

Biochemical analyses. Whole cell extracts were prepared in RIPA buffer and normalized for total protein or cell numbers before immunoblot analysis. Cytoplasmic and nuclear extracts from BMDMs and BMDCs were prepared by high salt extraction buffer (Buffer A: 10 mM HEPES pH 7.9, 10 mM KCl, 0.1 mM EGDA and 0.1 mM EDTA; Buffer C: 20 mM HEPES pH 7.9, 420 mM NaCl, 1.5 mM $MgCl_2$, 0.2 mM EDTA and 25% glycerol). Immunoprecipitation-immunoblotting analysis, EMSA, chromatin immunoprecipitation were performed as previously described[21,44]. In EMSAs focusing on RelB-DNA binding activity, nuclear extracts were ablated of RelA and c-Rel–containing DNA binding activities by preincubating them with RelA and c-Rel antibodies (**Fig. 3b** and **Supplementary Fig. 3b**). Similarly, nuclear extracts were preincubated with RelB and c-Rel antibodies when RelA DNA binding activity was the focus (**Fig. 3b**). Antibody-shift ablation analysis (for RelB, p50 and p52) was performed as previously described[22] and the specificities of antibodies were confirmed (**Supplementary Fig. 2e**).

Retrovirus-mediated gene transduction. RelB- or RelB-GFP expressing pBabe-puro constructs were generated by standard methods and transfected together with pCL.Eco into 293T cells with Lipofectamine 2000 transfection reagent (Invitrogen) for 48 h. Supernatant was filtered and used to infect MEFs. Transduced cells were selected with puromycin hydrochloride (Sigma). Images were acquired with a Zeiss Axio Z1 microscope.

Gene expression analysis. RNA extraction was performed with RNAeasy Mini Kit (Qiagen). RNA was collected from one set of time-course experiments (1 h, 8 h and 24 h) using wild-type (WT), *Relb*$^{-/-}$ and *Rel*$^{-/-}$*Relb*$^{-/-}$ BMDCs stimulated with 0.1 μM CpG (Invivogen) or 500 ng/ml Pam_3CSK_4. Labeling and hybridization to the Illumina v.2 gene expression chip was performed by UCSD Biogem core facility. The raw data were preprocessed and normalized by mloess method[45]. Genes differentially regulated between WT and *Rel*$^{-/-}$*Relb*$^{-/-}$ BMDCs during TLR stimulation time courses were analyzed by two-class paired SAM[46] implemented in the MeV program (multiple expression viewer)[47]. Class pairing was defined by corresponding time points between WT and *Rel*$^{-/-}$*Relb*$^{-/-}$ BMDCs. Differentially expressed genes identified at the false discovery rate below 5% were deemed significant. Genes with at least twofold induction during TLR-elicited DC maturation are listed in **Supplementary Table 1**. In heat maps, expression values of each gene were normalized to its maximum fold induction and clustered by hierarchical clustering with Euclidian distance (**Fig. 5e**). For phenotyping analyses (**Fig. 5f** and **Supplementary Table 2**), the average fold induction (FI)[26] in $\log_2$ scale across either timecourse (CpG and Pam_3CSK_4) was calculated for different genotypes, for example, FI_{WT}, $FI_{Rel-/-}$, and $FI_{Rel-/-Relb-/-}$. The RelB phenotype was defined as $FI_{WT}-FI_{Rel-/-}$, the c-Rel-RelB phenotype was defined as $FI_{WT}- FI_{Rel-/-Relb-/-}$. Quantitative (q)RT-PCR was performed after first-strand cDNA synthesis with oligo(dT) and SuperScript RT II (Invitrogen), using SYBR Green PCR Master Mix reagent (Stratagene), Eppendorf Mastercycler realplex system and gene-specific primers (**Supplementary Table 3**). Data analysis used the Δ(ΔCt) method with β-actin as normalization control to relate signals to those in MEFs or derive fold induction over basal levels. qRT-PCR and chromatin immunoprecipitation data shown are representative of three independent experiments (mean ± s.d.). Quantification of mRNA and protein abundance are representative of four independent experiments.

Computational modeling. The RelA–RelB mathematical model (version 5.0) involving mass action kinetic equations was developed based on a previously published model (version 3.1)[22] and experimental data[20] that allowed for constraints-based parameterization. Refinement of the model (version 5.1) and MEF- and DC-specific parameterization were based on experimental data presented in this paper. Computational simulations were performed in Matlab using the ode15s solver. Detailed descriptions are included in the **Supplementary Note**.

Statistics. Statistical significance was calculated by two-tailed Student's *t*-test with Prism software (GraphPad). Error bars were shown as either s.d. or s.e.m. as indicated.

42. Lutz, M.B. *et al.* An advanced culture method for generating large quantities of highly pure dendritic cells from mouse bone marrow. *J. Immunol. Methods* **223**, 77–92 (1999).
43. Boonstra, A. *et al.* Flexibility of mouse classical and plasmacytoid-derived dendritic cells in directing T helper type 1 and 2 cell development: dependency on antigen dose and differential toll-like receptor ligation. *J. Exp. Med.* **197**, 101–109 (2003).

44. Cheng, C.S. *et al.* The specificity of innate immune responses is enforced by repression of interferon response elements by NF-κB p50. *Sci. Signal.* **4**, ra11 (2011).
45. Sasik, R., Woelk, C.H. & Corbeil, J. Microarray truths and consequences. *J. Mol. Endocrinol.* **33**, 1–9 (2004).
46. Tusher, V.G., Tibshirani, R. & Chu, G. Significance analysis of microarrays applied to the ionizing radiation response. *Proc. Natl. Acad. Sci. USA* **98**, 5116–5121 (2001).
47. Saeed, A.I. *et al.* TM4 microarray software suite. *Methods Enzymol.* **411**, 134–193 (2006).

doi:10.1038/ni.2446

nature COMMUNICATIONS

OPEN

ARTICLE

Received 17 Apr 2012 | Accepted 18 Jun 2012 | Published 17 Jul 2012

DOI: 10.1038/ncomms1960

Epidermal phospholipase Cδ1 regulates granulocyte counts and systemic interleukin-17 levels in mice

Kaori Kanemaru[1,*], Yoshikazu Nakamura[1,*], Kojiro Sato[2], Ryota Kojima[1], Saori Takahashi[1], Mami Yamaguchi[1], Manabu Ichinohe[1], Hiroshi Kiyonari[3], Go Shioi[3], Kenji Kabashima[4], Kyoko Nakahigashi[4], Masataka Asagiri[5,6], Colin Jamora[7], Hideki Yamaguchi[8] & Kiyoko Fukami[1]

Phospholipase C is a key enzyme in phosphoinositide turnover. Although its functions have been extensively studied at the cellular level, many questions remain concerning its functions at the organ and individual animal levels. Here we demonstrate that mice lacking *phospholipase Cδ1* develop granulocytosis associated with elevated serum levels of the granulopoietic cytokine interleukin-17. Re-introduction of *phospholipase Cδ1* into keratinocytes of *phospholipase Cδ1*-deficient mice reverses this phenotype, whereas conditional ablation of *phospholipase Cδ1* in keratinocytes recreates it. Interleukin-17 and its key upstream regulator interleukin-23 are also upregulated in epidermis. Loss of *phospholipase Cδ1* from keratinocytes causes features of interleukin-17-associated inflammatory skin diseases. Phospholipase Cδ1 protein is downregulated in the epidermis of human psoriatic skin and in a mouse model of psoriasis. These results demonstrate that phosphoinositide turnover in keratinocytes regulates not only local inflammatory responses but also serum cytokine levels and systemic leukocyte counts, and affects distant haematopoietic organs.

[1] Laboratory of Genome and Biosignal, Tokyo University of Pharmacy and Life Sciences, Hachioji-shi, Tokyo 192-0392, Japan. [2] Department of Rheumatology and Applied Immunology, Faculty of Medicine, Saitama Medical University, Iruma-gun, Saitama 350-0495, Japan. [3] Laboratory for Animal Resources and Genetic Engineering, RIKEN Center for Developmental Biology, Kobe-shi, Hyogo 650-0047, Japan. [4] Department of Dermatology, Graduate School of Medicine, Kyoto University, Sakyo-ku, Kyoto 606-8507, Japan. [5] Department of Chemistry and Biochemistry, University of California San Diego, La Jolla, California 92093, USA. [6] Innovation Center for Immunoregulation and Therapeutics, Graduate School of Medicine, Kyoto University, Sakyo-ku, Kyoto 606-8501, Japan. [7] Section of Cell and Developmental Biology, Division of Biological Sciences, University of California San Diego, La Jolla, California 92093, USA. [8] Division of Metastasis and Invasion Signaling, National Cancer Center Research Institute, Chuo-ku, Tokyo 104-0045, Japan. *These authors contributed equally to this work. Correspondence and requests for materials should be addressed to Y.N. (email: ynakamur@toyaku.ac.jp) or to K.F. (email: kfukami@toyaku.ac.jp).

Phospholipase C (PLC) is a key enzyme in phosphoinositide turnover, an important signal transduction process in cells. PLC hydrolyses phosphatidylinositol 4,5-bisphosphate (PIP_2) to generate the second messengers inositol 1,4,5-trisphosphate (IP_3) and diacylglycerol (DAG), leading to elevated intracellular calcium ion concentrations and activation of protein kinase C (PKC)[1,2]. Although the functions of PLC have been extensively studied at the single-cell level[3], its physiological role in interactions among different cell types *in vivo* remains largely unknown.

Humoural factors communicate between different, distantly located cell types, and induce various physiological and cellular events such as inflammation, cell growth and apoptosis. Cytokines are one type of such humoural factors. Interleukin (IL)-17, also called IL-17A, is a pleiotropic cytokine that has emerged as a central player in the mammalian immune system, with important roles in the pathology of many disease processes, including allergic responses[4] and autoimmune diseases[5–10]. IL-17 is mainly produced by T lymphocytes under the regulation of IL-23 (refs 11,12), and in turn, regulates granulopoiesis through induction of granulocyte colony-stimulating factor (G-CSF)[13–15]. Granulocytes are key players in the pathogenesis of several inflammatory diseases. Increased baseline circulating granulocyte number is a risk factor for all-cause mortality and the progression of chronic diseases such as atherosclerosis and chronic renal failure[16–18].

We previously reported that one of the PLC isozymes, PLCδ1, was abundantly expressed in the epidermis[19] and that systemic loss of PLCδ1 resulted in epidermal hyperplasia associated with the infiltration of immune cells[20]. The epidermis is mainly composed of keratinocytes and is characterized by a polarized pattern of epithelial growth and differentiation, with a single basal layer of proliferating keratinocytes and multiple, overlying differentiated layers. Epidermal keratinocytes not only act as a barrier to the external environment, but also exert important functions in skin immune responses by secreting a variety of cytokines that initiate local inflammatory responses[21]. Indeed, keratinocytes have pivotal roles in the pathogenesis of human inflammatory skin diseases, including psoriasis and atopic dermatitis[22]. However, little is known about the ability of keratinocytes to regulate systemic inflammatory responses.

Here we demonstrate that loss of epidermal PLCδ1 results not only in skin inflammation associated with aberrant activation of IL-23/IL-17 axis, but also in systemic inflammation, characterized by increase in serum cytokine levels and systemic granulocytosis.

Results

Loss of systemic PLCδ1 causes granulocytosis. Loss of PLCβ3 in haematopoietic cells alters blood cell counts and populations in a haematopoietic cell intrinsic manner[23]. As PLCβ3 binds to PLCδ1 (ref. 24) in a manner similar to the binding of PLCβ2, we investigated if the systemic loss of PLCδ1 also affected blood cell counts and populations. Mice lacking the *PLCδ1* gene (*PLCδ1*$^{-/-}$ mice) exhibited a greater than twofold increase in peripheral blood leukocytes compared with wild-type mice (mean±s.e.m. cell numbers, $9.2\pm0.85\times10^6$ in wild-type versus $19\pm1.4\times10^6$ in *PLCδ1*$^{-/-}$ mice, $n=6$ for wild-type and $n=9$ for *PLCδ1*$^{-/-}$ mice). We also examined the population of CD11b$^+$ Gr-1$^+$ granulocytes. At first, we confirmed that *PLCδ1*$^{+/-}$ mice did not exhibit increase in granulocytes (Supplementary Fig. S1), and *PLCδ1*$^{+/-}$ mice were, therefore, used as a control in subsequent experiments. Granulocytes were markedly increased in the peripheral blood leukocyte in *PLCδ1*$^{-/-}$ mice, as well as in the spleen and bone marrow (Fig. 1a;

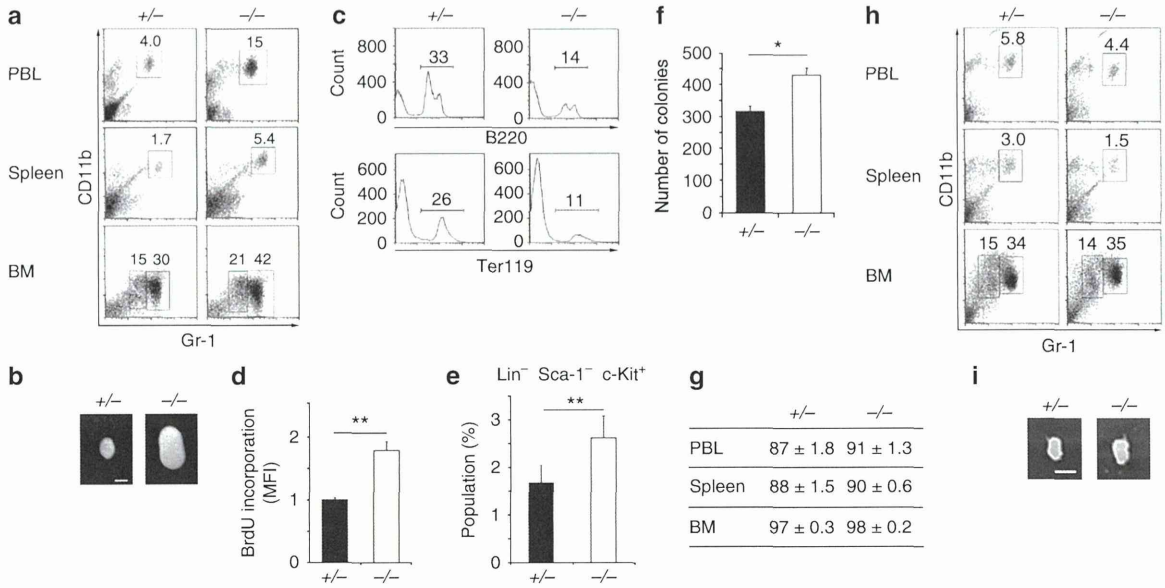

Figure 1 | *PLCδ1*$^{-/-}$ mice show granulocytosis in non-haematopoietic cell intrinsic manner. (**a**) Representative FACS profiles of CD11b$^+$ Gr-1$^+$ granulocytes in peripheral blood leukocytes (PBL), spleen, and bone marrow (BM) ($n=14$). Granulocytes in bone marrow were categorized into immature (CD11b$^+$ Gr-1^{low}) and mature (CD11b$^+$ Gr-1^{high}) subsets. (**b**) Macroscopic appearance of ILNs. Scale bar, 2 mm. (**c**) Representative FACS profiles of B220$^+$ and Ter119$^+$ cells in the BM ($n=7$–12). (**d**) BrdU incorporation in immature granulocytes (CD11b$^+$ Gr-1^{low}) in the BM. Data are expressed as the relative mean fluorescence intensity (MFI)±s.e.m. (MFI of *PLCδ1*$^{+/-}$ mice = 1) ($n=5$). (**e**) Populations of myeloid progenitor-rich Lin$^-$ Sca-1$^-$ c-Kit$^+$ cells in the BM. Mean±s.e.m. ($n=8$). (**f**) *In vitro* colony-forming assay. The numbers of colony-forming cells per 6×10^4 cells at 12 days after plating are displayed. Mean±s.e.m. ($n=4$). (**g**) Haematopoietic chimerism analysis. Chimerism of the PBL, spleen, and BM were determined in transplanted mice by FACS analysis of CD45.1$^-$ cells. Mean percentage±s.e.m. Six recipients in each group. Three donor mice per genotype were used. (**h**) Representative FACS profiles of CD45.1$^-$ CD11b$^+$ Gr-1$^+$ granulocytes in the PBL, spleen, and BM of CD45.1$^+$ congenic recipients reconstituted with *PLCδ1*$^{+/-}$ or *PLCδ1*$^{-/-}$ BM at 4 weeks post-transplantation. ($n=6$). Plots shown are gated on CD45.1$^-$ cells. (**i**) Macroscopic appearance of the ILNs. Scale bar, 2 mm. Mice used in all experiments were 8–12 weeks old. Statistical significance was assessed using a Student's *t*-test. *$P<0.05$; **$P<0.01$.

Table 1 | Absolute numbers of granulocytes, erythrocytes, and B and T lymphocytes in peripheral blood, spleen, bone marrow, and inguinal lymph nodes.

	Gr-1$^+$ CD11b$^+$	B220$^+$	Ter119$^+$	CD3$^+$
PBL				
PLCδ1$^{+/-}$	6.7±0.5 (*n*=6)	NA	NA	NA
PLCδ1$^{-/-}$	20.3±2.1** (*n*=9)	NA	NA	NA
Spleen				
PLCδ1$^{+/-}$	23±5.5 (*n*=10)	NA	NA	NA
PLCδ1$^{-/-}$	57±9.3** (*n*=10)	NA	NA	NA
BM				
PLCδ1$^{+/-}$	204±29 (*n*=12)	85±9.4 (*n*=12)	75±18 (*n*=7)	NA
PLCδ1$^{-/-}$	248±41* (*n*=12)	50±5.7* (*n*=12)	45±7.3* (*n*=7)	NA
ILNs				
PLCδ1$^{+/-}$	3.2±0.4 (*n*=5)	9.4±1.9 (*n*=4)	NA	40±1.0 (*n*=7)
PLCδ1$^{-/-}$	11.2±0.9** (*n*=5)	31.6±5.2** (*n*=4)	NA	81±1.6** (*n*=7)

NA, not available; PBL, peripheral blood lymphocytes; BM, bone marrow; INLs, inguinal lymph nodes.
Cell numbers are represented as number × 10^5 ±s.e.m.
For ILNs, Gr-1$^+$ cells were counted, instead of Gr-1$^+$ CD11b$^+$ cells.
Statistical significance was assessed using a Student's *t*-test.
*P<0.05.
**P<0.01.

Table 1). *PLCδ1*$^{-/-}$ mice also showed lymphadenopathy of the inguinal lymph nodes (ILNs) and mild splenomegaly (Fig. 1b; Supplementary Table S1). We confirmed that expression of other PLC isoforms was not affected by loss of PLCδ1 (Supplementary Fig. S2). Antibiotic treatment of *PLCδ1*$^{-/-}$ mice had no effect on the development of granulocytosis and lymphadenopathy (Supplementary Fig. S3a–d), and *PLCδ1*$^{-/-}$ granulocytes seemed to be morphologically and functionally normal (Supplementary Fig. S4a–c), suggesting that the observed granulocytosis was not a secondary effect of bacterial infection or impaired granulocyte function. Enhanced granulopoiesis in the bone marrow is often accompanied by a reduction of B lymphocytes and erythrocytes[25–27], and reduced numbers of B220$^+$ B lymphocytes and Ter119$^+$ erythrocytes were indeed observed in the bone marrow of *PLCδ1*$^{-/-}$ mice (Fig. 1c; Table 1). Granulocytes in mouse bone marrow can be categorized into immature and mature subsets[28], both of which were elevated in *PLCδ1*$^{-/-}$ bone marrow (Fig. 1a), suggesting that the increase in the granulocyte population arose from an immature progenitor population. A 5-bromo-2′-deoxy-uridine (BrdU) incorporation assay revealed that the proliferative activity of immature granulocytes was higher in *PLCδ1*$^{-/-}$ than in *PLCδ1*$^{+/-}$ bone marrow (Fig. 1d), suggesting that the increase in granulocyte number resulted from enhanced proliferation of immature granulocytes. An increased population of myeloid progenitor cells could also increase the granulocyte number in *PLCδ1*$^{-/-}$ mice. Indeed, the population of myeloid progenitor cells was greater in the bone marrow of *PLCδ1*$^{-/-}$ than of *PLCδ1*$^{+/-}$ mice (Fig. 1e), as was the number of myeloid colony-forming units (Fig. 1f), indicating that the loss of *PLCδ1* resulted in an increased population of myeloid progenitor cells in the bone marrow, possibly leading to granulocytosis.

As granulocytosis in *PLCδ1*$^{-/-}$ mice was likely caused by the lack of *PLCδ1* in the haematopoietic compartment, we generated mice lacking *PLCδ1* in the haematopoietic compartment by bone marrow transfer. Surprisingly, mice transplanted with *PLCδ1*$^{-/-}$ bone marrow did not develop granulocytosis or lymphadenopathy (Fig. 1g–i), indicating that the loss of *PLCδ1* in the haematopoietic system was not responsible for these phenotypes, and that the mechanism of granulocytosis in *PLCδ1*$^{-/-}$ mice differed from that in mice lacking PLCβ3 (ref. 23).

***PLCδ1*$^{-/-}$ mice display local and systemic IL-17 upregulation.** The granulocyte population was increased and the B220$^+$ B lymphocyte and Ter119$^+$ erythrocyte populations were decreased in the bone marrow of *PLCδ1*$^{-/-}$ mice (Fig. 1a,c; Table 1). However, the balance among colony-forming unit (CFU)- granulocyte/erythroid/macrophage/megakaryocyte, -granulocyte/macrophage, -macrophage, -granulocyte, and burst-forming unit-erythroid (BFU-E) was not dramatically disrupted in *PLCδ1*$^{-/-}$ bone marrow cells cultured *in vitro* (Supplementary Fig. S5). We therefore speculated that granulocytosis in *PLCδ1*$^{-/-}$ mice was induced by humoural factors secreted from peripheral tissues. IL-17 is a critical cytokine for granulopoiesis[13–15], and we, therefore, assessed serum IL-17 concentrations. IL-17 levels in the serum of control mice were below the detection limit, but those in *PLCδ1*$^{-/-}$ mice were detectable (Fig. 2a), indicating that circulating levels of the granulopoietic cytokine IL-17 were increased in *PLCδ1*$^{-/-}$ mice. The concentrations of other granulopoietic factors were not increased in *PLCδ1*$^{-/-}$ mice (Supplementary Fig. S6), strongly suggesting that IL-17 elevation is responsible for granulocytosis in these mice.

We investigated IL-17 production by lymphocytes in lymph nodes including ILNs and mesenteric lymph nodes (MLNs) by intracellular cytokine staining. The population of IL-17-producing cells was increased in ILNs, but not in MLNs, in *PLCδ1*$^{-/-}$ mice (Fig. 2b). The number of IL-17-producing cells in the ILNs of *PLCδ1*$^{-/-}$ mice exhibited a 3.9-fold increase compared with that in *PLCδ1*$^{+/-}$ mice (Fig. 2c). *IL-17* messenger RNA expression in ILNs, analysed using real-time RT–PCR was increased in *PLCδ1*$^{-/-}$ mice (Fig. 2d). We then investigated the specific cellular source of IL-17 in ILNs of *PLCδ1*$^{-/-}$ mice. Fluorescence-activated cell sorting (FACS) analysis revealed that the main producers of IL-17 were the γδ-T-cell receptor (TCR)-positive T cells (Fig. 2e). ILNs are skin-draining, whereas MLNs are not, suggesting that IL-17 was specifically upregulated in skin-draining lymph nodes. Indeed, another type of skin-draining lymph nodes, the axillary lymph nodes, also expressed high levels of *IL-17* mRNA (Fig. 2f). These results suggest that the skin system has a pivotal role in IL-17 upregulation. Importantly, *IL-17* expression was detected in *PLCδ1*$^{-/-}$ skin, but not in normal skin (Fig. 2g). In contrast to IL-17, the expression of *interferon γ* and *IL-4* was not increased in skin of *PLCδ1*$^{-/-}$ mice (Supplementary Fig. S7a). Thus, *PLCδ1*$^{-/-}$ mice showed IL-17 upregulation in skin and skin-draining lymph nodes.

Epidermal PLCδ1 is sufficient for normal IL-17 levels. Among skin cells, keratinocytes express the highest levels of PLCδ1 (ref. 19). In addition, IL-17 was upregulated in skin and skin-draining lymph nodes. We, therefore, hypothesized that the PLCδ1 in keratinocytes primarily regulates IL-17 levels. To test this hypothesis, we investigated whether reintroduction of *PLCδ1* into keratinocytes of *PLCδ1*$^{-/-}$ mice could restore normal IL-17 levels. We previously reported that expression of PLCδ1 in keratinocytes was mainly regulated by the transcription factor Foxn1 (ref. 29) and we, therefore, used a *Foxn1* promoter-driven *PLCδ1* gene (*Foxn1::PLCδ1*) (Fig. 3a) to restore PLCδ1 expression in *PLCδ1*$^{-/-}$ keratinocytes in a manner resembling that of endogenous *PLCδ1*. Mice carrying *Foxn1::PLCδ1* (Fig. 3b) appeared normal and did not exhibit any overt changes. Intercrossing *PLCδ1*$^{-/-}$ mice and mice carrying *Foxn1::*